Tunneling Valley Hall Effect Driven by Tilted Dirac Fermions

Shu-Hui Zhang [1,*] Ding-Fu Shao [2,†] Zi-An Wang [2,3] Jin Yang,[4] Wen Yang [4,‡] and Evgeny Y. Tsymbal[5,§]

[1]College of Mathematics and Physics, Beijing University of Chemical Technology, Beijing 100029, China
[2]Key Laboratory of Materials Physics, Institute of Solid State Physics, HFIPS, Chinese Academy of Sciences, Hefei 230031, China
[3]University of Science and Technology of China, Hefei 230026, China
[4]Beijing Computational Science Research Center, Beijing 100193, China
[5]Department of Physics and Astronomy & Nebraska Center for Materials and Nanoscience, University of Nebraska, Lincoln, Nebraska 68588-0299, USA

Valleytronics is a research field utilizing a valley degree of freedom of electrons for information processing and storage. A strong valley polarization is critical for realistic valleytronic applications. Here, we predict a tunneling valley Hall effect (TVHE) driven by tilted Dirac fermions in all-in-one tunnel junctions based on a two-dimensional (2D) valley material. Different doping of the electrode and spacer regions in these tunnel junctions results in momentum filtering of the tunneling Dirac fermions, generating a strong transverse valley Hall current dependent on the Dirac-cone tilting. Using the parameters of an existing 2D valley material, we demonstrate that such a strong TVHE can host a giant valley Hall angle even in the absence of the Berry curvature. Finally, we predict that resonant tunneling can occur in a tunnel junction with properly engineered device parameters such as the spacer width and transport direction, providing significant enhancement of the valley Hall angle. Our work opens a new approach to generate valley polarization in realistic valleytronic systems.

Valley, i.e., a local well-separated extremum of an energy band in the momentum space, has been recently identified as an additional degree of freedom carried by low-energy carriers [1–20]. To date, many material systems have been discovered exhibiting valleys in their band structure [21–23]. For example, in two-dimensional (2D) materials, such as graphene and transition metal dichalcogenides, there are two inequivalent valleys that occur at the K and $\bar{K}(-K)$ points at the edges of the Brillouin zone. In a doped system, an imbalance in carrier population between the K and $\bar{K}$ valleys, known as valley polarization, could be used to store binary information. However, the valleys at the reversed momenta, K and $\bar{K}$, in these materials are usually degenerate, which makes their polarization elusive.

Since K and $\bar{K}$ are connected by time reversal symmetry ($\hat{T}$), the perturbations breaking $\hat{T}$ symmetry, such as optical [6,24–33] and magnetic [29,34–44], have been employed to generate the valley polarization. These effects, though interesting, require large perturbative fields inaccessible for practical use. It was suggested that the large valley polarization can be induced in magnetic materials or heterostructures, where the spin and valley degrees of freedom are strongly coupled [45,46]. This mechanism, however, does not work for $\hat{T}$ invariant nonmagnetic materials.

Among the existing mechanisms, a valley Hall effect (VHE) allows the electrical generation of transverse valley dependent Hall currents [2]. This produces a detectable valley polarization in real space, while not breaking the valley degeneracy in k space. The intrinsic VHE is driven by the opposite-sign Berry curvatures at K and $\bar{K}$, leading to the opposite transverse velocities at the two valleys [2]. However, the Berry curvature only emerges in systems where the Kramers degeneracy is lifted, i.e., in nonmagnetic materials where space inversion ($\hat{P}$) symmetry is broken by a noncentrosymmetric structure or by the application of an electric field [47], or in magnetic materials, where $\hat{T}$ symmetry is broken by magnetism. It is sizable only in the semiconductors with very small band gaps. This limits the material choice for VHE and also demands a very strict control of the stoichiometry, as the doping effect can easily shift the Fermi energy (E_F) away from the band gap and significantly reduce the Berry curvature. It would be interesting from the fundamental point of view and desirable for valleytronic applications to find a new mechanism of VHE independent of the Berry curvature.

Here, we predict a Berry-curvature-free tunneling VHE (TVHE) produced by tilted Dirac fermions. The effect occurs in an all-in-one tunnel junction based on a 2D valley material where the valleys are described by the Hamiltonian supporting tilted Dirac fermions, and the electrodes and the spacer layer have different doping. We find that the tunneling Dirac fermions carry net transverse velocities opposite for K- and $\bar{K}$- valleys due to the momentum

filtering in the spacer layer controlled by the Dirac-cone tilting. This generates a strong TVHE with a giant valley Hall angle that is defined by the ratio of the valley Hall conductance and the longitudinal conductance. Finally, we predict that resonant tunneling can occur in a tunnel junction with properly engineered device parameters such as the spacer width and transport direction, providing significant enhancement of the valley Hall angle.

We consider a 2D material with valleys originating from an untilted [Fig. 1(a)] or tilted [Fig. 1(b)] Dirac cone at momenta K and $\bar{K}$ [Figs. 1(a) and 1(b)]. We assume an all-in-one tunnel junction based on this 2D valley material, which is divided into the left (L) and right (R) electrode regions and the central (C) spacer region. The electrodes are assumed to be n doped and the spacer p doped by voltage applied from the top and bottom gates. The valleys at the K and $\bar{K}$ points in this 2D material are described by the Dirac Hamiltonian [48]

$$H_{\eta,i}(\boldsymbol{q}) = \eta\mu_1\sigma_1 q_X + \mu_2\sigma_2 q_Y + \eta\mu_t\sigma_0 q_Y + V_i. \quad (1)$$

Here, index i denotes the left ($i = L$) or right ($i = R$) electrodes or the spacer ($i = C$). The Cartesian coordinate system X-Y is used, where the X (Y) axis is perpendicular
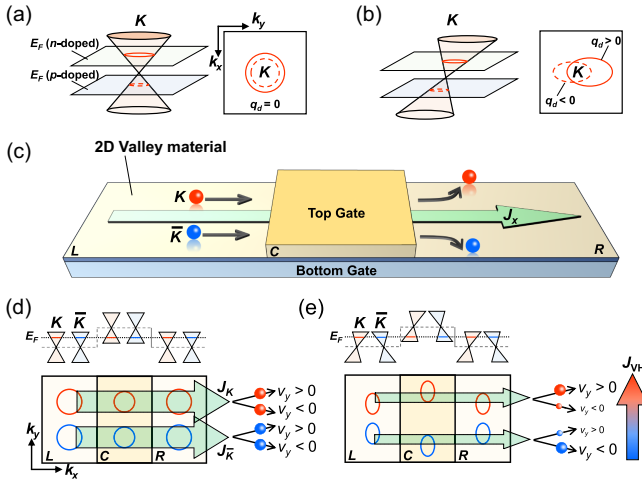

FIG. 1. (a),(b) Schematic electronic structure of a 2D material with a valley arising an untilted [(a), left] and tilted [(b), left] Dirac cone at the K point with respective Fermi surfaces of untilted [(a), right] and tilted [(b), right] Dirac fermions upon doping. (c) A schematic of the all-in-one tunnel junction representing left and right electrode regions separated by central spacer region. Top and bottom gates control doping in the electrodes and the spacer. A valley-neutral current J_x generates TVHE in the right electrode. (d),(e) The origin of the TVHE. For untilted Dirac cone valleys, the transverse electron velocities v_y at K and $\bar{K}$ are perfectly balanced, prohibiting the TVHE (d). For tilted Dirac cone valleys, electrons with negative (positive) transverse velocities v_y at K ($\bar{K}$) are largely filtered out, leading to a sizable TVHE and the associated transverse valley Hall current J_{VH} in the right electrode.

(parallel) to the tilt direction, $\eta = 1$ (-1) denotes the K- ($\bar{K}$-) valleys, $\boldsymbol{q} = (q_X, q_Y)$ is the wave vector with respect to K or $\bar{K}$, σ_1 and σ_2 are the Pauli matrices, σ_0 is the identity matrix, parameters μ_1, μ_2, and μ_t control the anisotropy and the tilt of the Dirac cone, and V_i are the potential associated with the doping effect.

In the absence of gate voltage ($V_i = 0$), the Dirac points are located at the Fermi level, $E_F = 0$, for all regions in the junction. In the presence of gate voltage, the Dirac point in region i is shifted to $E_F + V_i$ due to the doping effect produced by the gate voltage. When $\mu_1 = \mu_2$ and $\mu_t = 0$, the Dirac cone is not tilted, resulting in the isotropic Dirac fermions, as in graphene [49]. The associated Fermi surface is a circle centered at $q_X = q_Y = 0$. It changes size but does not shift upon doping [Fig. 1(a)]. When $\mu_t \neq 0$, the Dirac cone is tilted along the Y direction, resulting in type-I tilted Dirac fermions. The associated Fermi surface is an ellipse centered at $q = (0, \eta q_d)$. It changes size and shifts along the Y direction upon doping, with the shift q_d having opposite sign for n and p doping [Fig. 1(b)]. The type-I tilted Dirac fermions have been discussed for many 2D materials such as strained graphene [48], α-(BEDT-TTF)$_2$I$_3$ [50], 8-Pmmn borophene [51,52], and monolayer $1T'$-MX_2 (M = Mo, W, X = S, Se, Te) [53]. There can be also type-II Dirac fermions induced by strong tilting (e.g., [54]), which are not considered in this work since they cannot represent valleys as the Dirac points are not at the band extrema.

The longitudinal conductance is given by [55]

$$\sigma_{xx} = \frac{\sigma_0}{(2\pi)^2} \int \left(T^K_{q_y} + T^{\bar{K}}_{q_y} \right) dq_y, \quad (2)$$

where x (y) is the longitudinal (transverse) transport direction, $T^\eta_{q_y}$ is transmission for valley η at the transverse wave vector q_y, and $\sigma_0 = 2e^2/\hbar$. Hall conductance σ_{yx} and valley Hall conductance σ^V_{yx} in the right electrode are given by [56–61]

$$\sigma_{yx} = \sigma^K_{yx} + \sigma^{\bar{K}}_{yx}, \quad \sigma^V_{yx} = \sigma^K_{yx} - \sigma^{\bar{K}}_{yx}, \quad (3)$$

where σ^η_{yx} is the conductance associated with the valley-dependent transverse current J^η_y

$$\sigma^\eta_{yx} = \frac{\sigma_0}{(2\pi)^2} \int \zeta^{\eta,\rightarrow}_{q_y} T^\eta_{q_y} dq_y, \quad (4)$$

where $\zeta^{\eta,\rightarrow}_{q_y} = (v^{\eta,\rightarrow}_{y,q_y}/v^{\eta,\rightarrow}_{x,q_y})$. Here $v^{\eta,\rightarrow}_{r,q_y}$ denotes the longitudinal ($r = x$) and transverse ($r = y$) band velocities of the right-going ($\rightarrow$) states in the electrode. The Hall angle $\Theta = \sigma_{yx}/\sigma_{xx}$ and valley Hall angle $\Theta_V = \sigma^V_{yx}/\sigma_{xx}$ can be then defined to estimate the strengths of these effects. We set $E_F = 0$ and assume that the left and the right electrodes are n doped with $V_L = V_R = -V_0$, and the central region is p doped with $V_C = V_0$. In the ballistic transport regime

with negligible intervalley scattering and conserved wave vector [62–64], and $T_{q_y}^\eta$ is determined by matching the Fermi surfaces in the electrodes and the spacer. When the tilt direction Y is perpendicular to the longitudinal transport direction [Fig. 1(b)], the Fermi surface of valley η is symmetric with respect to $q_y = \eta q_d$, resulting in $v_{x,q_y}^{\eta,\to} = v_{x,q_y'}^{\eta,\to}$ and $v_{y,q_y}^{\eta,\to} = -v_{y,q_y'}^{\eta,\to}$, where $q_y' = 2\eta q_d - q_y$. This leads to $\zeta_{q_y}^{\eta,\to} = -\zeta_{q_y'}^{\eta,\to}$. Therefore, the distribution of $T_{q_y}^\eta$ determines σ_{yx}^η.

In the absence of tilting, the valley Fermi surfaces are perfectly circular with different sizes in the electrode and spacer regions due to different doping, as shown in Figs. 1(a) and 1(d). Since the origin of these Fermi surfaces does not change with doping ($q_d = 0$), the tunneling barrier height for Dirac fermions is momentum and valley independent, resulting in $T_{q_y}^K = T_{-q_y}^K = T_{q_y}^{\bar{K}} = T_{-q_y}^{\bar{K}}$. Therefore, the transmitted Dirac fermions have zero net transverse velocities, for both total current J_x and valley-dependent current J_x^η, resulting in zero Hall and valley Hall conductances [Fig. 1(d)].

In contrast, in the presence of tilting, the Fermi surfaces of Dirac fermions are shifted and elongated along the y (Y) direction, as shown in Figs. 1(b) and 1(e). Since the displacement of the Fermi surfaces in the electrodes and the spacer are opposite in sign due to reverse (n and p) doping, the tunneling barrier height is momentum dependent, resulting in *momentum filtering* that creates disbalance between the tunneling Dirac fermions at q_y and q_y' at each valley, leading to $T_{q_y}^\eta \neq T_{q_y'}^\eta$ and hence the finite valley-dependent transverse current J_y^η. However, for tilting along the y (Y) direction, each valley is symmetric with respect to $q_x = 0$ and hence $v_{x,q_y}^{\eta,\to} = -v_{x,q_y}^{\eta,\leftarrow}$ and $v_{y,q_y}^{\eta,\to} = v_{y,q_y}^{\eta,\leftarrow}$, where $\leftarrow$ denotes the left-going state. In addition, the two valleys are connected by $\hat{T}$ symmetry so that $v_{x,q_y}^{K,\to} = -v_{x,-q_y}^{\bar{K},\leftarrow}$, $v_{y,q_y}^{K,\to} = -v_{y,-q_y}^{\bar{K},\leftarrow}$ and hence $\zeta_{q_y}^{K,\to} = -\zeta_{-q_y}^{\bar{K},\to}$. $\hat{T}$ symmetry also enforces $T_{q_y}^K = T_{-q_y}^{\bar{K}}$ and thus $\sigma_{yx}^K = -\sigma_{yx}^{\bar{K}}$, resulting in the valley-dependent transverse currents opposite in sign, $J_y^K = -J_y^{\bar{K}}$. Therefore, a nonzero valley Hall current $J_{VH} = J_y^K - J_y^{\bar{K}} = 2J_y^K$ is expected with the valley Hall conductance given by

$$\sigma_{yx}^V = \frac{2\sigma_0}{(2\pi)^2} \int \zeta_{q_y}^{K,\to} T_{q_y}^K dq_y. \tag{5}$$

Because of $\zeta_{q_y}^{\eta,\to} = -\zeta_{q_y'}^{\eta,\to}$, a nonzero σ_{yx}^V occurs if $T_{q_y}^K \neq T_{q_y'}^K$, which is expected for a tilted Dirac cone.

Next, we quantitatively demonstrate TVHE by performing quantum-transport calculations for a realistic tunnel junction. We first consider $\mu_1 = \mu_2 = \mu_F = 10^6$ m/s and $\mu_t = 0$, corresponding to isotropic Dirac fermions in graphene [49], and assume central region width $w = 10$ nm
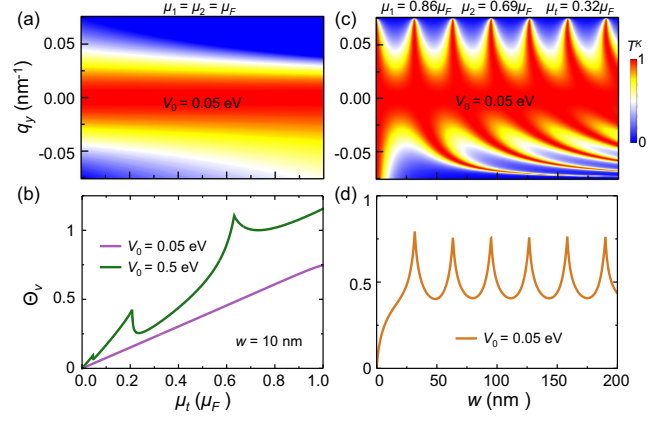

FIG. 2. (a),(b) Transmission $T_{q_y}^K$ for valley K as a function of q_y (a) and valley Hall angle Θ_V as a function μ_t (b) for $w = 10$ nm. (c),(d) Transmission $T_{q_y}^K$ (c) and Θ_V valley Hall angle (d) as functions of w. The parameters used in the calculations are indicated.

and low doping of $V_0 = 0.05$ eV. As expected, we find that $T_{q_y}^K$ is symmetric with respect to $q_y = 0$ [Fig. 2(a) for $\mu_t = 0$], leading to vanishing σ_{yx} and σ_{yx}^V. For nonzero μ_t, transmission $T_{q_y}^K$ becomes asymmetric with respect to q_y [Fig. 2(a) for $\mu_t > 0$], which implies $T_{q_y}^K \neq T_{q_y'}^K$ giving rise to a finite σ_{yx}^V [Fig. 2(b)]. For a weak tilting of $\mu_t = 0.2 \, \mu_F$, we obtain a sizable valley Hall angle $\Theta_V = 0.15$. Θ_V can be further enhanced by increasing μ_t [Fig. 2(b)].

For high doping of $V_0 = 0.5$ eV, we find a much larger Θ_V. This is expected as the increase of V_0 shifts the Fermi surfaces stronger upon doping and thus enhances momentum filtering asymmetry between q_y and q_y' at each valley and thus J_y^K and $J_{VH} = 2J_y^K$ [Fig. 1(e)]. Interestingly, we find that the Θ_V-versus-μ_t curve exhibits anomalous peaks [Fig. 2(b)]. Such peaks originate from resonant tunneling due to the matching of the spacer width w and the longitudinal electronic wavelength λ_x in the spacer region, such that $w = 0.5 n\lambda_x$, where n is an integer, $\lambda_x = 2\pi/q_x$, and $q_x = (1/\mu_1)\sqrt{(E_F - V_C - \mu_t q_y)^2 - \mu_2^2 q_y^2}$ [65].

The emergence of resonant tunneling implies a possibility to realize a strong VHE with a low doping and moderate tilting. Here, we consider parameters $\mu_1 = 0.86 \, \mu_F$, $\mu_2 = 0.69 \, \mu_F$, and $\mu_t = 0.32 \, \mu_F$ corresponding to 2D valley material 8-*Pmmn* borophene [52], and calculate $T_{q_y}^K$ and Θ_V as functions of w. For a low doping of $V_0 = 0.05$ eV, we find that the distribution of $T_{q_y}^K$ exhibits a "fishbone" pattern [Fig. 2(c)], which has typical peaks reflecting the resonant tunneling. For example, for $q_y = 0.05$ nm^{-1}, the resonant enhancements occur at $w = 0.5 n\lambda_x \approx 32 n$ nm, as can be seen from Fig. 2(c). As a result, a large $\Theta_V \approx 0.75$ is predicted for certain widths of the spacer layer w [Fig. 2(d)].
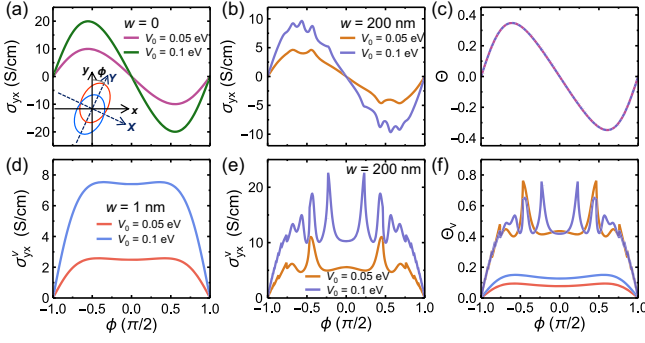
FIG. 3. (a),(b) Hall conductance σ_{yx} as a function of angle ϕ for $w = 0$ (a) and 200 nm (b) for $V_0 = 0.05$ and 0.1 eV. (c) Hall angle Θ as a function of ϕ for the parameters as in (a) and (b). (d), (e) Valley Hall conductance σ_{yx}^{V} as a function of ϕ for $w = 1$ nm (d) and 200 nm (e). (f) Valley Hall angle Θ_V as a function of ϕ for the parameters as in (d) and (e).

We further consider a more general case where the tilting Y direction has an angle ϕ away from the transverse y direction [inset in Fig. 3(a)], using the parameters for 8-$Pmmn$ borophene [52]. Experimentally, the angle ϕ can be controlled by changing the direction of the longitudinal current. We choose the central region widths w such that they do not support resonant tunneling and calculate Hall conductance σ_{yx} as a function of ϕ for different V_0. For $\phi \neq 0.5n\pi$ (n is an integer), we find that the symmetry constraint $\sigma_{yx}^K = -\sigma_{yx}^{\bar{K}}$ is absent, resulting in a finite σ_{yx} even for a uniform system [$w = 0$, Fig. 3(a)]. This is due to the fact that at $\mu_1 \neq \mu_2$, $\sigma_{xx}(\phi = 0) \neq \sigma_{xx}(\phi = 0.5\pi)$ resulting in $\sigma_{yx}(\phi) = [\sigma_{xx}(0.5\pi) - \sigma_{xx}(0)] \sin\phi\cos\phi$. When w is large, resonant tunneling appears and leads to peaks in σ_{yx} [Fig. 3(b)]. Interestingly, although w and V_0 strongly influence the σ_{yx}-ϕ curve, the calculated Hall

angles Θ are the same for different w and V_0, and the features of resonant tunneling are not revealed in Θ [Fig. 3(c)]. On the contrary, the valley Hall conductance σ_{yx}^{V} arises only at nonzero w and $\phi \neq 0.5 m\pi$ (m is an odd number) [Figs. 3(d) and 3(e)] and increases with increasing V_0. For a small w, the σ_{yx}^{V}-ϕ curves are smooth [Fig. 3(d)], while for a large w, pronounced peaks associated with resonant tunneling emerge [Fig. 3(e)]. These peaks also appear in the Θ_V-ϕ curves [Fig. 3(f)]. Therefore, transport direction can also be used to control resonant tunneling for enhancing Θ_V. This is different from that in the ordinary Hall effect (OHE) and the AHE in bulk materials, where the Hall current is usually independent of the current direction, but is similar to that in the in-plane AHE discovered recently, where the Hall current is strongly dependent on the relative direction of the longitudinal current and an in-plane magnetic field [66,67].

The different behaviors of Θ and Θ_V shown in Figs. 3(c) and 3(f) can be understood from a simple analytic derivation. Since the two valleys are connected by $\hat{T}$ symmetry, we have $\mathcal{T}_{q_y} \equiv T_{q_y}^K = T_{-q_y}^{\bar{K}}$ and $v_{r,q_y}^{K,\rightarrow} = -v_{r,-q_y}^{\bar{K},\leftarrow}$ (where $\leftarrow$ denotes the left-going state). The latter results in $\zeta_{q_y}^{K,\rightarrow} = \zeta_{-q_y}^{\bar{K},\leftarrow}$. We can then define $\vartheta_{\pm} = \zeta_{q_y}^{K,\rightarrow} \pm \zeta_{q_y}^{K,\leftarrow}$ and rewrite Eq. (3) as follows:

$$\sigma_{yx} = \frac{\sigma_0}{(2\pi)^2}\int \mathcal{T}_{q_y}\vartheta_+ dq_y,$$

$$\sigma_{yx}^{V} = \frac{\sigma_0}{(2\pi)^2}\int \mathcal{T}_{q_y}\vartheta_- dq_y. \tag{6}$$

Introducing parameters $\gamma_1 = \mu_2/\mu_1$ and $\gamma_2 = \mu_t/\mu_1$ to reflect the anisotropy and tilting, respectively, we obtain [68]

$$\vartheta_+ = \frac{2\sin\phi\cos\phi(\gamma_1^2 - \gamma_2^2 - 1)}{\cos^2\phi + (\gamma_1^2 - \gamma_2^2)\sin^2\phi},$$

$$\vartheta_- = \frac{(\gamma_2 V_0\mu_1\cos\phi + (\gamma_1^2 - \gamma_2^2)q_y\mu_1^2)(q_x^{\leftarrow} - q_x^{\rightarrow})}{(\gamma_1^2 - \gamma_2^2)q_y^2\mu_1^2 + 2\gamma_2 V_0\mu_1(\cos\phi + 1) - (\cos^2\phi + \gamma_1^2\sin^2\phi)V_0^2}. \tag{7}$$

It is seen that ϑ_+ is a function of γ_1, γ_2, ϕ and does not depend on w, V_0, and q_y. As a result, the Hall angle takes a universal form

$$\Theta \equiv \frac{\sigma_{yx}}{\sigma_{xx}} = \frac{\sin\phi\cos\phi(\gamma_1^2 - \gamma_2^2 - 1)}{\cos^2\phi + (\gamma_1^2 - \gamma_2^2)\sin^2\phi}, \tag{8}$$

consistent with our numerical result in Fig. 2(c). On the other hand, ϑ_- is dependent on V_0 and q_y. This leads to Θ_V being dependent on w and V_0, as shown in Fig. 3(f).

The predicted TVHE is related to the previously proposed tunneling anomalous and spin Hall effects [56–61]. Both effects are associated with the momentum filtering. However, the origins of the momentum filtering for these effects are different. The tunneling anomalous and spin Hall effects occur due to the symmetry mismatch in a magnetic electrode, where $\hat{T}$ symmetry is broken, and a nonmagnetic barrier layer with strong spin-orbit coupling, where $\hat{T}$ symmetry is preserved [56–61]. On the contrary, for the TVHE, the momentum filtering is due to the mismatch of the Fermi surfaces of the tilted Dirac fermions

in the electrode and spacer regions resulting from reverse. The symmetry remains the same for all regions of such a tunnel junction, and hence the junction can be constructed using a single 2D material (Fig. 1), where the doping, the spacer width, and the transport direction can be conveniently controlled.

The proposed TVHE has significant advantages over the intrinsic VHE driven by the Berry curvature mechanism. First, the intrinsic VHE occurs only in materials with broken $\hat{P}\hat{T}$ symmetry. The proposed TVHE, on the other hand, does not have these restrictions, and thus can emerge even in centrosymmetric nonmagnets or spin-degenerate antiferromagnets with preserved $\hat{P}\hat{T}$ symmetry. Second, the strong intrinsic VHE normally requires E_F to be close to the Weyl points or at the band edge with not too large spin splitting [62,63,75], while the proposed TVHE exhibits a giant valley Hall angle that can be further optimized by engineering the parameters of the junction such as Dirac cone tilting, doping, spacer width, and transport direction.

The TVHE is expected to occur not only for the reversly doped electrodes and spacer ($V_L = V_R = -V_C$), as was assumed above, but for any modulated doping along the junction. As long as $V_L = V_R \neq V_C$, a nonvanishing transverse valley current emerges and produces the TVHE. We note here that although we consider a tunnel junction with the abrupt potential changes at the interfaces, our conclusions are also valid for the potential smoothly changing across the interfaces, as discussed in Supplemental Material [68]. The presence of regions with inhomogeneous doping and tilting may produce stronger intervalley scattering that is expected to affect the predicted TVHE, which is worth investigating in future.

Finally, the proposed TVHE device can be made nonvolatile. In a heterostructure where the 2D valley material is placed on top of a ferroelectric insulator, different doping of the electrodes and the spacer layer can be induced by polarization charges of oppositely polarized ferroelectric domains, and the TVHE can be controlled by ferroelectric switching.

In conclusion, we have predicted a TVHE driven by the tilted Dirac fermions in an all-in-one tunnel junction based on a 2D valley material. Different doping of the electrodes and the spacer layer in this tunnel junction results in tilting-dependent momentum filtering of the tunneling Dirac fermions, generating a strong TVHE with a giant valley Hall angle. Resonant tunneling is predicted to occur in the tunnel junction with properly engineered device parameters, such as the spacer width and transport direction, providing significant enhancement of the valley Hall angle. Our work opens a new approach to generate valley polarization in realistic valleytronic systems.

    *shuhuizhang@mail.buct.edu.cn
    †dfshao@issp.ac.cn
    ‡wenyang@csrc.ac.cn
    §tsymbal@unl.edu

[1] A. Rycerz, J. Tworzydło, and C. W. J. Beenakker, Valley filter and valley valve in graphene, Nat. Phys. **3**, 172 (2007).

[2] D. Xiao, W. Yao, and Q. Niu, Valley-contrasting physics in graphene: Magnetic moment and topological transport, Phys. Rev. Lett. **99**, 236809 (2007).

[3] I. Martin, Y. M. Blanter, and A. F. Morpurgo, Topological confinement in bilayer graphene, Phys. Rev. Lett. **100**, 036804 (2008).

[4] J. L. Garcia-Pomar, A. Cortijo, and M. Nieto-Vesperinas, Fully valley-polarized electron beams in graphene, Phys. Rev. Lett. **100**, 236801 (2008).

[5] Z. Wu, F. Zhai, F. M. Peeters, H. Q. Xu, and K. Chang, Valley-dependent Brewster angles and Goos-Hänchen effect in strained graphene, Phys. Rev. Lett. **106**, 176802 (2011).

[6] D. Xiao, G.-B. Liu, W. Feng, X. Xu, and W. Yao, Coupled spin and valley physics in monolayers of MoS_2 and other group-VI dichalcogenides, Phys. Rev. Lett. **108**, 196802 (2012).

[7] Y. Jiang, T. Low, K. Chang, M. I. Katsnelson, and F. Guinea, Generation of pure bulk valley current in graphene, Phys. Rev. Lett. **110**, 046601 (2013).

[8] R. V. Gorbachev, J. C. W. Song, G. L. Yu, A. V. Kretinin, F. Withers, Y. Cao, A. Mishchenko, I. V. Grigorieva, K. S. Novoselov, L. S. Levitov, and A. K. Geim, Detecting topological currents in graphene superlattices, Science **346**, 448 (2014).

[9] Y. Shimazaki, M. Yamamoto, I. V. Borzenets, K. Watanabe, T. Taniguchi, and S. Tarucha, Generation and detection of pure valley current by electrically induced Berry curvature in bilayer graphene, Nat. Phys. **11**, 1032 (2015).

[10] M. Sui, G. Chen, L. Ma, W.-Y. Shan, D. Tian, K. Watanabe, T. Taniguchi, X. Jin, W. Yao, D. Xiao, and Y. Zhang, Gate-tunable topological valley transport in bilayer graphene, Nat. Phys. **11**, 1027 (2015).

[11] K. F. Mak, K. L. McGill, J. Park, and P. L. McEuen, The valley Hall effect in MoS_2 transistors, Science **344**, 1489 (2014).

[12] J. Lee, K. F. Mak, and J. Shan, Electrical control of the valley Hall effect in bilayer MoS_2 transistors, Nat. Nanotechnol. **11**, 421 (2016).

[13] H. Pan, Z. Li, C.-C. Liu, G. Zhu, Z. Qiao, and Y. Yao, Valley-polarized quantum anomalous Hall effect in silicene, Phys. Rev. Lett. **112**, 106802 (2014).

[14] H. Yu, Y. Wu, G.-B. Liu, X. Xu, and W. Yao, Nonlinear valley and spin currents from Fermi pocket anisotropy in 2D crystals, Phys. Rev. Lett. **113**, 156603 (2014).

[15] M. Settnes, S. R. Power, M. Brandbyge, and A.-P. Jauho, Graphene nanobubbles as valley filters and beam splitters, Phys. Rev. Lett. **117**, 276801 (2016).

[16] X.-T. An, J. Xiao, M. W.-Y. Tu, H. Yu, V. I. Fal'ko, and W. Yao, Realization of valley and spin pumps by scattering at nonmagnetic disorders, Phys. Rev. Lett. **118**, 096602 (2017).

[17] J. Zhou, Q. Sun, and P. Jena, Valley-polarized quantum anomalous Hall effect in ferrimagnetic honeycomb lattices, Phys. Rev. Lett. **119**, 046403 (2017).

[18] C. Hu, V. Michaud-Rioux, W. Yao, and H. Guo, Moiré valleytronics: Realizing dense arrays of topological helical channels, Phys. Rev. Lett. **121**, 186403 (2018).

[19] Z.-M. Yu, S. Guan, X.-L. Sheng, W. Gao, and S. A. Yang, Valley-layer coupling: A new design principle for valleytronics, Phys. Rev. Lett. **124**, 037701 (2020).

[20] T. Zhou, S. Cheng, M. Schleenvoigt, P. Schüffelgen, H. Jiang, Z. Yang, and I. Žutić, Quantum spin-valley Hall kink states: From concept to materials design, Phys. Rev. Lett. **127**, 116402 (2021).

[21] J. R. Schaibley, H. Yu, G. Clark, P. Rivera, J. S. Ross, K. L. Seyler, W. Yao, and X. Xu, Valleytronics in 2D materials, Nat. Rev. Mater. **1**, 16055 (2016).

[22] S. A. Vitale, D. Nezich, J. O. Varghese, P. Kim, N. Gedik, P. Jarillo-Herrero, D. Xiao, and M. Rothschild, Valleytronics: Opportunities, challenges, and paths forward, Small **14**, 1801483 (2018).

[23] S. Zhao, X. Li, B. Dong, H. Wang, H. Wang, Y. Zhang, Z. Han, and H. Zhang, Valley manipulation in monolayer transition metal dichalcogenides and their hybrid systems: Status and challenges, Rep. Prog. Phys. **84**, 026401 (2021).

[24] G. Sallen, L. Bouet, X. Marie, G. Wang, C. R. Zhu, W. P. Han, Y. Lu, P. H. Tan, T. Amand, B. L. Liu, and B. Urbaszek, Robust optical emission polarization in MoS_2 monolayers through selective valley excitation, Phys. Rev. B **86**, 081301 (2012).

[25] K. F. Mak, K. He, J. Shan, and T. F. Heinz, Control of valley polarization in monolayer MoS_2 by optical helicity, Nat. Nanotechnol. **7**, 494 (2012).

[26] T. Cao, G. Wang, W. Han, H. Ye, C. Zhu, J. Shi, Q. Niu, P. Tan, E. Wang, B. Liu, and J. Feng, Valley-selective circular dichroism of monolayer molybdenum disulphide, Nat. Commun. **3**, 887 (2012).

[27] H. Yu, Y. Wang, Q. Tong, X. Xu, and W. Yao, Anomalous light cones and valley optical selection rules of interlayer excitons in twisted heterobilayers, Phys. Rev. Lett. **115**, 187002 (2015).

[28] A. Kundu, H. A. Fertig, and B. Seradjeh, Floquet-engineered valleytronics in Dirac systems, Phys. Rev. Lett. **116**, 016802 (2016).

[29] G. Wang, X. Marie, B. L. Liu, T. Amand, C. Robert, F. Cadiz, P. Renucci, and B. Urbaszek, Control of exciton valley coherence in transition metal dichalcogenide monolayers, Phys. Rev. Lett. **117**, 187401 (2016).

[30] R. Bertoni, C. W. Nicholson, L. Waldecker, H. Hübener, C. Monney, U. De Giovannini, M. Puppin, M. Hoesch, E. Springate, R. T. Chapman, C. Cacho, M. Wolf, A. Rubio, and R. Ernstorfer, Generation and evolution of spin-, valley-, and layer-polarized excited carriers in inversion-symmetric WSe_2, Phys. Rev. Lett. **117**, 277201 (2016).

[31] G. Wang, C. Robert, M. M. Glazov, F. Cadiz, E. Courtade, T. Amand, D. Lagarde, T. Taniguchi, K. Watanabe, B. Urbaszek, and X. Marie, In-plane propagation of light in transition metal dichalcogenide monolayers: Optical selection rules, Phys. Rev. Lett. **119**, 047401 (2017).

[32] Z. Ye, D. Sun, and T. F. Heinz, Optical manipulation of valley pseudospin, Nat. Phys. **13**, 26 (2017).

[33] K. F. Mak, D. Xiao, and J. Shan, Light-valley interactions in 2D semiconductors, Nat. Photonics **12**, 451 (2018).

[34] C. J. Tabert and E. J. Nicol, Valley-spin polarization in the magneto-optical response of silicene and other similar 2D crystals, Phys. Rev. Lett. **110**, 197402 (2013).

[35] Y. Li, J. Ludwig, T. Low, A. Chernikov, X. Cui, G. Arefe, Y. D. Kim, A. M. van der Zande, A. Rigosi, H. M. Hill, S. H. Kim, J. Hone, Z. Li, D. Smirnov, and T. F. Heinz, Valley splitting and polarization by the Zeeman effect in monolayer $MoSe_2$, Phys. Rev. Lett. **113**, 266804 (2014).

[36] D. MacNeill, C. Heikes, K. F. Mak, Z. Anderson, A. Kormányos, V. Zólyomi, J. Park, and D. C. Ralph, Breaking of valley degeneracy by magnetic field in monolayer $MoSe_2$, Phys. Rev. Lett. **114**, 037401 (2015).

[37] S.-G. Cheng, H. Liu, H. Jiang, Q.-F. Sun, and X. C. Xie, Manipulation and characterization of the valley-polarized topological kink states in graphene-based interferometers, Phys. Rev. Lett. **121**, 156801 (2018).

[38] R. Kraft, I. V. Krainov, V. Gall, A. P. Dmitriev, R. Krupke, I. V. Gornyi, and R. Danneau, Valley subband splitting in bilayer graphene quantum point contacts, Phys. Rev. Lett. **121**, 257703 (2018).

[39] H. Overweg, A. Knothe, T. Fabian, L. Linhart, P. Rickhaus, L. Wernli, K. Watanabe, T. Taniguchi, D. Sánchez, J. Burgdörfer, F. Libisch, V. I. Fal'ko, K. Ensslin, and T. Ihn, Topologically nontrivial valley states in bilayer graphene quantum point contacts, Phys. Rev. Lett. **121**, 257702 (2018).

[40] X.-X. Zhang, Y. Lai, E. Dohner, S. Moon, T. Taniguchi, K. Watanabe, D. Smirnov, and T. F. Heinz, Zeeman-induced valley-sensitive photocurrent in monolayer MoS_2, Phys. Rev. Lett. **122**, 127401 (2019).

[41] H. Takenaka, S. Sandhoefner, A. A. Kovalev, and E. Y. Tsymbal, Magnetoelectric control of topological phases in graphene, Phys. Rev. B **100**, 125156 (2019).

[42] Y.-W. Liu, Z. Hou, S.-Y. Li, Q.-F. Sun, and L. He, Movable valley switch driven by Berry phase in bilayer-graphene resonators, Phys. Rev. Lett. **124**, 166801 (2020).

[43] S.-Y. Li, Y. Su, Y-N. Ren, and L. He, Valley polarization and inversion in strained graphene via pseudo-Landau levels, valley splitting of real Landau levels, and confined states, Phys. Rev. Lett. **124**, 106802 (2020).

[44] Y. Lee, A. Knothe, H. Overweg, M. Eich, C. Gold, A. Kurzmann, V. Klasovika, T. Taniguchi, K. Wantanabe, V. Fal'ko, T. Ihn, K. Ensslin, and P. Rickhaus, Tunable valley splitting due to topological orbital magnetic moment in bilayer graphene quantum point contacts, Phys. Rev. Lett. **124,** 126802 (2020).

[45] W.-Y. Tong, S.-J. Gong, X. Wan, and C.-G. Duan, Concepts of ferrovalley material and anomalous valley Hall effect, Nat. Commun. **7,** 13612 (2016).

[46] H. Y. Ma, M. Hu, N. Li, J. Liu, W. Yao, J.-F. Jia, and J. Liu, Multifunctional antiferromagnetic materials with giant piezomagnetism and noncollinear spin current, Nat. Commun. **12,** 2846 (2021).

[47] L. L. Tao and E. Y. Tsymbal, Two-dimensional spin-valley locking spin valve, Phys. Rev. B **100,** 161110(R) (2019).

[48] M. O. Goerbig, J.-N. Fuchs, G. Montambaux, and F. Piéchon, Tilted anisotropic Dirac cones in quinoid-type graphene and $\alpha - (\text{BEDT-TTF})_2 I_3$, Phys. Rev. B **78,** 045415 (2008).

[49] A. H. Castro Neto, F. Guinea, N. M. R. Peres, K. S. Novoselov, and A. K. Geim, The electronic properties of graphene, Rev. Mod. Phys. **81,** 109 (2009).

[50] S. Katayama, A. Kobayashi, and Y. Suzumura, Pressure-induced zero-gap semiconducting state in organic conductor $\alpha - (\text{BEDT-TTF})_2 I_3$ salt, J. Phys. Soc. Jpn. **75,** 054705 (2006).

[51] X.-F. Zhou, X. Dong, A. R. Oganov, Q. Zhu, Y. Tian, and H.-T. Wang, Semimetallic two-dimensional boron allotrope with massless Dirac fermions, Phys. Rev. Lett. **112,** 085502 (2014).

[52] A. D. Zabolotskiy and Y. E. Lozovik, Strain-induced pseudomagnetic field in the Dirac semimetal borophene, Phys. Rev. B **94,** 165403 (2016).

[53] X. Qian, J. Liu, L. Fu, and J. Li, Quantum spin Hall effect in two-dimensional transition metal dichalcogenides, Science **346,** 1344 (2014).

[54] L. L. Tao and E. Y. Tsymbal, Two-dimensional type-II Dirac fermions in a $\text{LaAlO}_3/\text{LaNiO}_3/\text{LaAlO}_3$ quantum well, Phys. Rev. B **98,** 121102 (2018).

[55] S. Datta, *Electronic Transport in Mesoscopic Systems* (Cambridge University Press, Cambridge, England, 1995).

[56] A. Vedyayev, N. Ryzhanova, N. Strelkov, and B. Dieny, Spontaneous anomalous and spin Hall Effects due to spin-orbit scattering of evanescent wave functions in magnetic tunnel junctions, Phys. Rev. Lett. **110,** 247204 (2013).

[57] A. V. Vedyayev, M. S. Titova, N. V. Ryzhanova, M. Y. Zhuravlev, and E. Y. Tsymbal, Anomalous and spin Hall effects in a magnetic tunnel junction with Rashba spin-orbit coupling, Appl. Phys. Lett. **103,** 032406 (2013).

[58] A. Matos-Abiague and J. Fabian, Tunneling anomalous and spin Hall effects, Phys. Rev. Lett. **115,** 056602 (2015).

[59] M. Y. Zhuravlev, A. Alexandrov, L. L. Tao, and E. Y. Tsymbal, Tunneling anomalous Hall effect in a ferroelectric tunnel junction, Appl. Phys. Lett. **113,** 172405 (2018).

[60] B. Scharf, A. Matos-Abiague, J. E. Han, E. M. Hankiewicz, and I. Žutić, Tunneling planar Hall effect in topological insulators: Spin valves and amplifiers, Phys. Rev. Lett. **117,** 166806 (2016).

[61] D.-F. Shao, S.-H. Zhang, R.-C. Xiao, Z.-A. Wang, W. J. Lu, Y. P. Sun, and E. Y. Tsymbal, Spin-neutral tunneling anomalous Hall effect, Phys. Rev. B **106,** L180404 (2022).

[62] Z. Wu, B. T. Zhou, X. Cai, P. Cheung, G.-B. Liu, M. Huang, J. Lin, T. Han, L. An, Y. Wang, S. Xu, G. Long, C. Cheng, K. T. Law, F. Zhang, and N. Wang, Intrinsic valley Hall transport in atomically thin MoS_2, Nat. Commun. **10,** 611 (2019).

[63] J. Chen, Y. Zhou, J. Yan, J. Liu, L. Xu, J. Wang, T. Wan, Y. He, W. Zhang, and Y. Chai, Room-temperature valley transistors for low-power neuromorphic computing, Nat. Commun. **13,** 7758 (2022).

[64] The intervalley scattering is ignored in the calculation, since the typical scale of this scattering in 2D valley materials lies in the micrometer range which is well beyond the width of the central region in the considered tunnel junction, as shown in Refs. [62,63].

[65] S.-B. Zhang, C.-A. Li, F. Peña-Benitez, P. Surówka, R. Moessner, L. W. Molenkamp, and B. Trauzettel, Super-resonant transport of topological surface states subjected to in-plane magnetic fields, Phys. Rev. Lett. **127,** 076601 (2021).

[66] J. Zhou *et al.*, Heterodimensional superlattice with in-plane anomalous Hall effect, Nature (London) **609,** 46 (2022).

[67] This is because the "driving force" of the OHE and AHE, i.e., a magnetic field or a net magnetization, is usually out-of-plane and always perpendicular to the longitudinal current. On the contrary, the TVHE proposed here is driven by the Dirac cone tilting along the in-plane direction, and hence the relative direction of the current and tilting axis strongly influences Θ_V.

[68] See Supplemental Material at http://link.aps.org/supplemental/10.1103/PhysRevLett.131.246301 for the detailed analytical derivations of the transmission probability, tunneling Hall effects, and the numerical calculations for a tunneling junction with a smooth potential, where Refs. [69–74] are cited.

[69] K. Sadhukhan and A. Agarwal, Anisotropic plasmons, Friedel oscillations, and screening in $8 - Pmmn$ borophene, Phys. Rev. B **96,** 035410 (2017).

[70] S. F. Islam and A. M. Jayannavar, Signature of tilted Dirac cones in Weiss oscillations of $8 - Pmmn$ borophene, Phys. Rev. B **96,** 235405 (2017).

[71] S.-H. Zhang and W. Yang, Oblique Klein tunneling in $8 - Pmmn$ borophene $p - n$ junctions, Phys. Rev. B **97,** 235440 (2018).

[72] Y.-F. Zhou, H. Jiang, X. C. Xie, and Q.-F. Sun, Two-dimensional lattice model for the surface states of topological insulators, Phys. Rev. B **95,** 245137 (2017).

[73] R. Logemann, K. J. A. Reijnders, T. Tudorovskiy, M. I. Katsnelson, and S. Yuan, Modeling Klein tunneling and caustics of electron waves in graphene, Phys. Rev. B **91,** 045420 (2015).

[74] C. W. Groth, M. Wimmer, A. R. Akhmerov, and X. Waintal, Kwant: A software package for quantum transport, New J. Phys. **16,** 063065 (2014).

[75] C. Jiang, A. Rasmita, H. Ma, Q. Tan, Z. Zhang, Z. Huang, S. Lai, N. Wang, S. Liu, X. Liu, T. Yu, Q. Xiong, and W.-B. Gao, A room-temperature gate-tunable bipolar valley Hall effect in molybdenum disulfide/tungsten diselenide heterostructures, Nat. Electron. **5,** 23 (2022).

[76] M. A. Caprio, LevelScheme: A level scheme drawing and scientific figure preparation system for Mathematica, Comput. Phys. Commun. **171,** 107 (2005).